Zbynek Heger[1,2]
Jan Zitka[1]
Natalia Cernei[1,2]
Sona Krizkova[1,2]
Marketa Sztalmachova[2,3]
Pavel Kopel[1,2]
Michal Masarik[2,3]
Petr Hodek[4]
Ondrej Zitka[1,2]
Vojtech Adam[1,2]
Rene Kizek[1,2]

[1]Department of Chemistry and Biochemistry, Mendel University, Brno, Czech Republic
[2]Central European Institute of Technology, Brno University of Technology, Brno, Czech Republic
[3]Department of Pathological Physiology, Faculty of Medicine, Masaryk University, Brno, Czech Republic
[4]Department of Biochemistry, Faculty of Science, Charles University in Prague, Prague, Czech Republic

Received November 25, 2014
Revised February 4, 2015
Accepted February 8, 2015

Research Article

3D-printed biosensor with poly(dimethylsiloxane) reservoir for magnetic separation and quantum dots-based immunolabeling of metallothionein

Currently, metallothioneins (MTs) are extensively investigated as the molecular biomarkers and the significant positive association of the MT amount was observed in tumorous versus healthy tissue of various types of malignant tumors, including head and neck cancer. Thus, we proposed a biosensor with fluorescence detection, comprising paramagnetic nanoparticles (nanomaghemite core with gold nanoparticles containing shell) for the magnetic separation of MT, based on affinity of its sulfhydryl groups toward gold. Biosensor was crafted from PDMS combined with technology of 3D printing and contained reservoir with volume of 50 μL linked to input (sample/detection components and washing/immunobuffer) and output (waste). For the immunolabeling of immobilized MT anti-MT antibodies conjugated to CdTe quantum dots through synthetic heptapeptide were employed. After optimization of fundamental conditions of the immunolabeling (120 min, 20°C, and 1250 rpm) we performed it on a surface of paramagnetic nanoparticles in the biosensor reservoir, with evaluation of fluorescence of quantum dots (λ_{exc} 400 nm, and λ_{em} 555 nm). The developed biosensor was applied for quantification of MT in cell lines derived from spinocellular carcinoma (cell line 122P-N) and fibroblasts (122P-F) and levels of the biomarker were found to be about 90 nM in tumor cells and 37 nM in fibroblasts. The proposed system is able to work with low volumes ($<$ 100 μL), with low acquisition costs and high portability.

Keywords:
Biosensor / Bioseparation / Head and neck cancer / Metallothionein / Nanotechnology
DOI 10.1002/elps.201400559

1 Introduction

A biomarker is a substance found in a biological fluid or in tissues that indicates the presence of an abnormal condition. If the biomarker is a protein or metabolite, it can either be present at a higher or lower amount than what is considered a normal range. The detection of cancer biomarkers plays a fundamental role not only in diagnosis, but also in classification of tumor development, assessment of prognosis, and treatment success rate [1]. Despite a long list of candidates with a prognostic and predictive ability that can be found in the literature, not one of them has been widely accepted for routine application in managing patients with spinocellular carcinoma [2]. However, it was described that low-molecular-mass (6000–8000 Da) intracellular proteins—metallothioneins (MTs), involved in numerous physiological and pathophysiological processes such as intracellular storage, transport and metabolism of metal ions, exhibit significant potential in prediction of spinocellular carcinomas development, related to the tumor grade and patients survival rate [3–5].

Moreover, MTs are expressed inducibly as a response to oxidative stress [6] and the biosynthesis of MT was shown to be elevated to protect the cells against cytotoxicity [7], radiation, and/or DNA damage [8].

Hence, the development of biosensors providing an accurate, sensitive, and specific detection, together with portability and the ability to furnish continuous real time signals of MT levels in bodily fluids can be highly interesting for screening diagnostic purposes. According to the definition, firmly established in the analytical field "biosensor" is a detection system that relies on a biomolecule for molecular recognition

Correspondence: Dr. Rene Kizek, Department of Chemistry and Biochemistry, Mendel University in Brno, Zemedelska 1, CZ-613 00 Brno, Czech Republic
E-mail: kizek@sci.muni.cz
Fax: +420-5-4521-2044

Abbreviations: DPV, differential pulse voltammetry; **MT**, metallothionein; **QD**, quantum dot; **RBC**, red blood cell

Colour Online: See the article online to view Figs. 1–4 in colour.

and a transducer to produce an observable output [9]. MTs can be specifically recognized by using anti-MT antibodies [2, 10], which provide a possibility to be further bioconjugated with nanoscale particles, such as quantum dots (QDs) [11].

In the present study, MT was isolated from rabbit liver (MT was induced by intraperitoneal injection of 10 mg of $CdCl_2$ kg^{-1} of weight) by using fast-protein LC and further employed as an immunogen to produce the anti-MT antibodies. Thus obtained antibodies were further bioconjugated through heptapeptide linker to CdTe QDs (herein after QDs@Anti-MTAbs) and the entire bioconjugate was utilized as a recognition element in 3D-printed biosensor with fluorescence detection of MT, immobilized on a surface of paramagnetic nanoparticles. Entire isolation and immunolabeling was carried out in a poly(dimethylsiloxane) reservoir, enabling excitation of QDs by LED with subsequent evaluation of their emission, which was transmitted by optical fibers to a photodiode with multifunction amplifier. By using the proposed biosensor, similar sensitivity was achieved when compared to the conventional ELISA. Finally, the biosensor was employed to quantify MT content in the spinocellular carcinoma cell lines and the experimental results are reported.

2 Materials and methods

2.1 Chemical compounds

All the reagents for syntheses, native oligonucleotides, standards, and other chemicals were purchased from Sigma-Aldrich (St. Louis, MO, USA) in ACS purity, unless noted otherwise.

2.2 MT isolation

MT was isolated from the rabbit liver and purified by using fast-protein liquid chromatography according to our previous study [12]. The purity was evaluated by using MALDI-TOF/TOF (Bruker ultrafleXtreme, Bruker Daltonik, Germany).

2.3 Production of anti-MT antibodies

The chickens were immunized with MT (MT2 isoform) and IgY fractions with reactivity to MT2 were collected from the egg yolk. The obtained IgY were purified by the immunoaffinity chromatography and the final concentration of proteins was established to be 54.7 mg/mL. The antibodies in 135 mM PBS were stabilized by 0.1% sodium azide. The immunoreactivity of produced antibodies was tested in our previous studies [13, 14]. The entire process was conducted in accordance with the Regulations for the Care and Use of Laboratory Animals (311/1997, Ministry of Agriculture, Czech Republic).

2.4 Synthesis of paramagnetic nanoparticles, quantum dots, and synthetic peptide

Nanometric maghemite core was prepared by $NaBH_4$ reduction of $FeCl_3 \bullet 6H_2O$, according to the following protocol: 1 g of $FeCl_3 \bullet 6H_2O$ (3.7 mM) was dissolved in 80 mL of MilliQ water and a solution of 0.2 g of $NaBH_4$ (5.3 mM) in ammonia (3.5% *w/v*, 10 mL) was poured into the first solution under vigorous stirring. The obtained solution was boiled for 2 h. After cooling down the magnetic nanoparticles were separated by external magnetic field and washed with water for several times. Subsequently, nanomaghemite particles were suspended in an aqueous solution of 20 mL of 7.5% PVP (40 μM) and mixed with 25 mL of 1 mM $HAuCl_4$ followed by addition of 0.75 mL of 0.1 M trisodium citrate to produce a shell structure. Resulting mixture was stirred overnight, separated using an external magnetic force field and dried at 40°C. CdTe QDs were prepared according to workflow published in our previous study [15]. The heptapeptide with the amino acid sequence HWRGWVC (943.0912 Da) was prepared on Liberty Blue peptide synthesizer (CEM, Matthews, NC, USA) by standard fluorenylmethyloxycarbonyl solid-phase synthesis, using 20% piperidine in DMF (*v/v*) for deprotection. The purity of crude peptide was analyzed using HPLC-UV (ESA, Chelmsford, MA, USA) and MALDI-TOF/TOF.

2.5 Characterization of nanoscaled synthetic products

The morphology of the paramagnetic nanoparticles was characterised by electron microscope FEG-SEM MIRA XMU (Tescan, a.s., Brno, Czech Republic), according to [16]. Nanoparticles size and ζ-potential were measured by Particle Size Analyzer (Zetasizer Nano ZS90, Malvern instruments, Malvern, UK). Particles were dispersed in 135 mM PBS (pH 7.4) and incubated at 25°C for 15 min prior the measurements. Elemental composition of core-shell nanoparticles was investigated by using X-ray fluorescence using Xepos (SPECTRO analytical instruments, Kleve, Germany), following conditions published in our previous study [17]. QDs were characterized by mean of fluorescence behaviour using fluorescence spectrometer Tecan Infinite 200 PRO (TECAN, Maennedorf, Switzerland). All the measurements were performed at 25°C. The photographs of QDs were taken under UV light illumination (Vilber Lourmat, Marne-la-Vallée, France), using $\lambda = 254$ nm. For testing the immunocompatibility, the immuno-buffers were prepared according to [18].

2.6 Enzyme-linked immunosorbent assay of MT

The bottom of the ELISA plate (Nunc MaxiSorp®, Sigma-Aldrich) was firstly coated with 100 μL of MT and incubated (1 h, 37°C) in a thermostat. After five-times repeated washing with washing buffer (135 mM PBS-Tween-20), anti-MT antibodies were added and bottom of ELISA plate was

blocked by 150 μL of 1% BSA (30 min, 37°C). After another five washing steps with washing buffer addition (100 μL) of primary antibody (anti-MTAbs, 1:500 in 0.1% BSA in 135 mM PBS) followed and incubation was performed (2 h, 37°C). After washing (PBS-Tween-20), 100 μL of secondary antibody (anti-chicken Abs, 1:30 000 in 0.1% BSA in 135 mM PBS) was added and solution was incubated (1 h, 37°C). After washing, 100 μL of 1.2 mM chromogenic substrate 3,3′,5,5′-tetramethylbenzidine was added (15 min incubation) and finally 50 μL of stop solution (0.5 M H_2SO_4) was added. Absorbance was determined immediately by using a microplate reader Tecan Infinite 200 PRO (TECAN) at 450 nm.

2.7 Preparation of red blood cells for enzyme-linked immunosorbent assay of MT

The red blood cells (RBC) were obtained through centrifugation, using a Microcentrifuge 5417R (Eppendorf AG) under 2000 g at 4°C for 5 min. Obtained pellet, composed of RBC was mixed with cold distilled water (1:1.4) and put into −80°C, to disrupt the RBC. The sample prepared by this manner was further utilized for ELISA.

2.8 Preparation of MT-nanoparticles and Abs@QDs conjugates

Prior to a conjugation, paramagnetic nanoparticles (0.5 mg/100 μL) were washed in borate buffer (pH = 6) to remove impurities. For bioconjugation 500 nM MT was used and the resulting mixture (1:1) was incubated for 30 min at 800 rpm and 20°C in a thermoblock ThermomixerR (Eppendorf AG, Hamburg, Germany). After the incubation, the conjugate of MT and nanoparticles was washed three times using borate buffer (pH = 6), by using external magnetic field and stored (4°C) for further experiments. To assure the proper orientation of antibodies, localized on the surface of QDs, the synthetic heptapeptide HWRGWVC was employed as a linker between Abs and QD according to our previous study [11].

2.9 Evaluation of MT binding on nanoparticles surface

Quantification of MT bound on the surface of paramagnetic nanoparticles was carried out using differential pulse voltammetry (DPV), using parameters according to [15]. The recovery of MT binding was calculated as a difference between applied and detected concentration of MT.

2.10 MT immunolabeling

The immunolabeling of MT, immobilized on the surface of nanoparticles (100 μL of nanoparticles dispersion), was carried out through QDs@anti-MTAbs (100 μL, 500 μg/mL of total protein in pH 6 borate buffer with 1% BSA). Mixtures were taken together in ratio 1:1 and subsequently incubated by using thermoblock Thermomixer® R (Eppendorf AG), while the ideal conditions of incubation (time, temperature, revolutions per minute) were optimized. After the incubation, an unbound residue, comprising QDs@anti-MTAbs was removed using the external magnetic field. Nanoparticles-MT-QDs@anti-MTAbs complex was washed three times with 50 mM borate buffer (pH = 6) and prepared for fluorescence measurements.

2.11 Fluorescence measurements

Fluorescence analyses were performed using multifunctional microplate reader Tecan Infinite 200 PRO (TECAN). Samples (50 μL) were applied into the UV-transparent 96 well microtitration plate with flat bottom Costar® (Corning, NY, USA). All measurements were performed at 25°C controlled by Tecan Infinite 200 PRO (TECAN). The quantification of MT was carried out at $\lambda_{exc} = 400$ nm and fluorescence intensity at $\lambda_{em} = 510$ nm was evaluated.

2.12 Fabrication of 3D-printed biosensor device with PDMS chip

The platforms for PDMS chip (reservoir volume of 50 μL), excitation, emission filters and optical fibres were crafted by using 3D-printing technology (acrylonitrile butadiene styrene as material) by using 3D printer PROFI3DMAKER (Aroya, Straznice, Czech Republic). PDMS (Sylgard 184, Dow Corning, Midland, MI, USA) was evacuated prior to use to remove the unwanted air bubbles. LED (λ = 400 nm; Roithner LaserTechnik, Vienna, Austria) was employed as an excitation light source. Emission bandpass filter (λ = 550(55) nm) and excitation shortpass filter (λ = 425 nm) were purchased from Semrock (Rochester, NY, USA). Optical fibres (UV-Vis transparent) were obtained from Edmund optics (Barrington, NJ, USA). A control unit Arduino linked to the LED driver controlled the system. The signal from UV-Vis photodiode S3991-01 (Hamamatsu Photonics, Hamamatsu, Japan) was evaluated by multifunction two-channel amplifier board (Digi board, Sglux, Berlin, Germany). All other technical details can be found in [19].

2.13 Cell lines and their preparation for measurements

Tumor tissue material (biopsies from Department of head and neck surgery, St. Anne's Faculty Hospital in Brno) was placed into the culture medium (RPMI 1640, Biochrom US, Holliston, MA, USA) with an addition of antibiotic-antimycotic solution, gentamycin sulfate and ciprofloxacin (Santa Cruz Biotechnology, Dallas, TX, USA) to prevent bacteria, fungi, and yeast contamination. The material was

kept cold and was transferred to the laboratory as fast as possible. Within the sterile environment and after rinsing the sample by 70% EtOH, the most viable tissue was selected and any necrotic tissue was discarded. Tissue was mechanically dissociated into small pieces. For digestion by proteolytic enzymes was used trypsin protocol as follows: The small tissue fragments were added and stirred into the sterile 135 mM PBS and centrifuged at 4°C, 2700 rpm for 7 min. The cell pellet was resuspended into 0.25% trypsin in the RPMI 1640 medium and left overnight at 4°C. Then medium was removed and tissue was incubated at 37°C for 30 min. The cell pellet was resuspended in the medium with an addition of antibiotic-antimycotic solution, gentamycin sulfate, ciprofloxacin, and 10% fetal bovine serum. Primary cell lines were cultivated at 37°C and 5% CO_2 in the humidified atmosphere up to 50% confluence. For separation of the cancer cells from the fibroblasts, magnetic particles MidiMACS™ Starting Kit (CD44 MicroBeads- human, FcR Blocking Reagent- human, LS Columns, Miltenyi Biotec, Bergisch Gladbach, Germany) were used. Cells adhered to the flask bottom were grown in complete medium until they reach 70% confluence, after that they were passaged. For experiments, two experimental cell lines were employed, named 212P-N (spinocellular carcinoma) and 122P-F (fibroblasts), derived from second patient.

After harvest, cells were frozen by liquid nitrogen to disrupt their structure. The frozen sample was further homogenized using ultrasonic homogenizer SONOPLUS mini20 (Bandelin electronic, Berlin, Germany). Subsequently, 1 mL of 0.2 M phosphate buffer (pH, 7.0) was added and the sample was homogenized for 5 min. The homogenate was further centrifuged using Microcentrifuge 5417R under the following conditions at 4°C for 15 min. Finally, the supernatant was filtered through a membrane filter (0.45-μm nylon filter disc; Millipore, Billerica, MA, USA) and used for electrochemical measurements and in-chip direct ELISA, following conditions, described above (Sections 2.8 and 2.10).

2.14 Descriptive statistics

Mathematical analysis of the data and their graphical interpretation were realized by Microsoft Excel®, Microsoft Word®, and Microsoft PowerPoint®. Results are expressed as mean ± SD unless noted otherwise. The LODs (3 S/N) were calculated according to Long and Winefordner [20], whereas *N* was expressed as a SD of noise determined in the signal domain after five measurements of blank sample (ACS water).

3 Results and discussion

3.1 Basic characterization of synthetic nanoscaled product and subsequent conjugation

The iron oxide nanoparticles (γ-Fe_2O_3 and Fe_3O_4) are versatile nanoscaled material, applicable for the magnetic separation of various types of analytes [16, 19], in particular due to possibility of surface modifications, which leads to introduction of a broad spectrum of binding sites. With information, that MT sulfhydryl groups exhibit stronger affinity toward Au than Zn or Cd [22], we employed γ-Fe_2O_3 core for surface modification with PVP and chloroauric acid ($HAuCl_4$), while its reduction with citric acid in PVP leads to the formation of extremely stable gold nanoparticles-polymer nanocomposites on the γ-Fe_2O_3 core [21]. Resulting nanoparticles can be conveniently immobilized via external magnetic field.

To obtain insight into the properties of synthetic nanoparticles, basic characterization was carried out, including examination of their morphology by using the scanning electron microscopy (Fig. 1A). As it is shown, spherical-shaped nanoparticles aggregated (length of scale bar 200 nm), despite the fact that their ζ-potential was established to −22 ± 1.3 mV (Fig. 1B), which is close to bare iron oxides absolute ζ-potential (−30 mV) [23], pointing at stable dispersion. The nanoparticles suspension consisted of particles with size distribution range 30–145 nm, with the most abundant size about approximately 44 ± 8 nm (24% of nanoparticles; Fig. 1B). By using X-ray fluorescence, it was revealed that iron formed almost one-half of present elements (451 μg/mg), while gold was present in amount of 156 μg/mg of dry nanoparticles (Fig. 1C). Rest of nanoparticles mass was probably formed by other organic elements (H, O, C); however, further elemental analyses will be required for confirmation.

The CdTe QDs as a second nanotechnological utility were employed in our experiment due to their excellence in the exceptional brightness and high quantum yield [24]. Thus, they can be helpful in development of highly sensitive fluorescence biosensors (reviewed in [25]). Metal nature of QDs offers also electrochemical detection [26]. QDs are size-tunable in their preparation workflow, which results in products with different fluorescence behaviour. We have prepared QDs with excitation maxima $\lambda_{exc} = 400$ nm (Fig. 1D) and emission maxima $\lambda_{em} = 510$ nm (inset in Fig. 1D, showing the fluorescence intensity on applied QDs concentration in range 0–800 μg/mL). With an idea of immunolabeling of immobilized MT, QDs had to be modified with the synthetic heptapeptide (HWRGWVC), working as a spacer for site-directed conjugation with the anti-MT antibodies. This approach was successfully employed in our previous study dealing with bioconjugation of QDs with immunoglobulins [11]. Oriented conjugation is known to provide nanoprobes with a higher specificity when compared to random conjugation using carbodiimide chemistry [27]. As it can be seen in Fig. 1E the bioconjugation resulted in product, exhibiting two emission maxima ($\lambda_{em =}$ 300 and 510 nm), when applying $\lambda_{exc} = 245$ nm. This phenomenon is caused by presence of both - QDs and heptapeptide, containing two fluorescent tryptophans (W) in its sequence. From Fig. 1F it is obvious, that bioconjugation with peptide lead to slight decrease of QDs fluorescence (about 21%). After application of anti-MT antibodies, QDs-HWR conjugate tended to retain its fluorescence intensity (decrease about 9%), while significant shift into higher emission

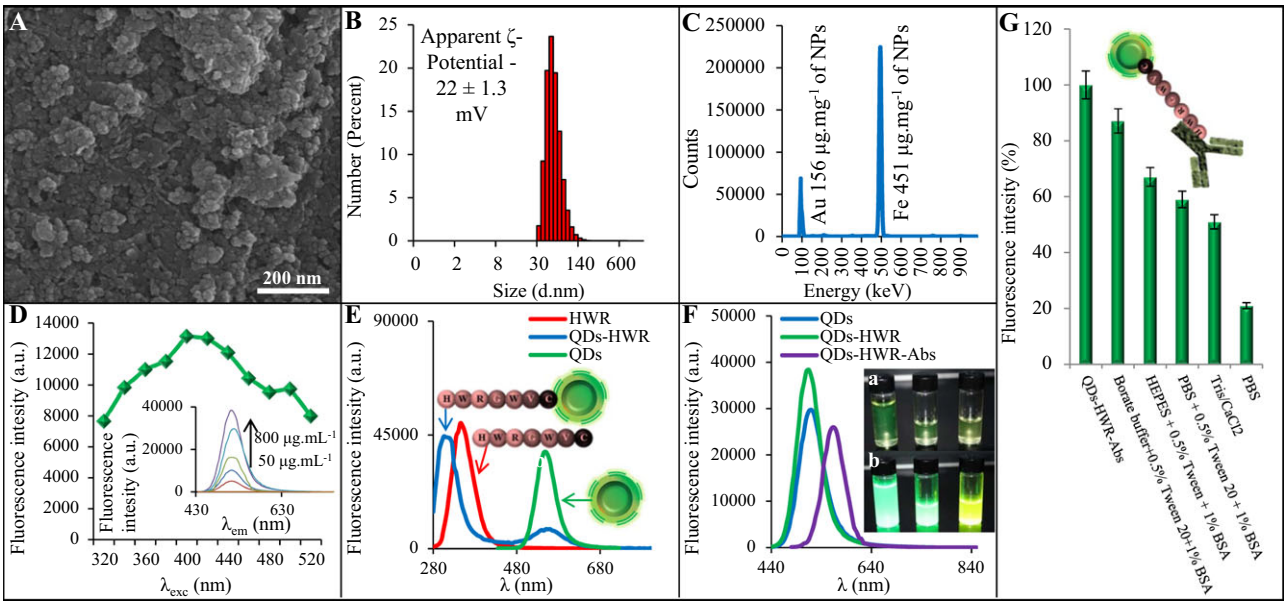

Figure 1. The characterization of magnetic nanoparticles expressed as: (A) SEM micrograph (length of scale bar is 200 nm), (B) Particles size distribution, with expression of their zeta potential. (C) X-ray fluorescence spectra, showing the major elemental composition. (D) Expression of dependence of fluorescence intensity of CdTE QDs (100 μg/mL) in ideal emission (λ_{em} = 510 nm) on applied excitation wavelength (determined in range 320–520 nm). Inserted are emission spectra of CdTe QDs in concentrations 50, 100, 200, 400, and 800 μg/mL. (E) Emission spectra showing the fluorescence behavior of QDs-HWR complex by using the excitation of tryptophan (λ_{exc} = 245 nm), obtained in HWR heptapeptide sequence. For comparison, spectra of HWR (10 μg/mL, λ_{exc} = 245 nm) and QDs (800 μg/mL, λ_{exc} = 400 nm) are provided. (F) Fluorescence spectra, showing shift in emission after modification of QDs-HWR with antibodies (applied λ_{exc} = 400 nm). Inserted are photos of QDs, QDs functionalized with HWR heptapeptide and QDs with HWR and anti-MT antibodies (from left to right), obtained in (a) ambient light and (b) under UV illumination (λ = 254 nm). (G) Optimization of immuno-buffers (pH 7.4, or unbuffered control with pH 7.0) for antigen-antibody binding and their suitability to do not quench the fluorescence of QDs-HWR-Abs. Fluorescence was determined at λ_{em} = 555 nm.

maxima was observed (λ_{em} = 555 nm), visible also by naked eye as a slight color change to yellow (Fig. 1Fa and Fb). Finally, resulting product (QDs@Anti-MTAbs) was tested for compatibility with common immunobuffers (pH 7.4, instead of unbuffered control sample with in ACS water with pH 7.0; Fig. 1G). Generally, QDs suffer from fluorescence instability in buffers, probably due to interaction with their components, leading to induction of QDs colloidal instability and subsequent quenching [18]. The highest fluorescence was achieved by using borate buffer with 0.5% Tween-20 and 1% BSA (fluorescence reduction about 13%, when compared with QDs@anti-MTAbs). All buffers, containing BSA were more compatible with QDs fluorescence, since BSA helps to stabilize it, regardless of the QDs surface chemistry (amine-terminated, streptavidin-coated or antibody-conjugated) [18].

3.2 Conventional ELISA and nanoparticles-based immunolabeling of MT

After characterization of the behaviour of employed nanoparticles, further steps lead us to optimize the conditions for direct MT ELISA (entire workflow process is depicted in Fig. 2A), which was carried out by using anti-MT antibodies as the primary Abs and anti-chicken Abs as the enzyme-linked secondary Abs. As it is shown in Fig. 2B, the calibration curve for MT was established in linear dynamic range of 1.3–100.0 nM with following parameters: $y = 0.0002x + 0.068$, $R^2 = 0.9612$. To show the functionality of anti-MT Abs in real sample analyses, we have employed it to quantify MT in disrupted RBC (Fig. 2C) in different dilutions (1:50; 1:100; 1:200; 1:400 of PBS buffer) and we have determined MT in all of them in relatively similar amount (55–71 nM). Similarly to immobilization of MT on the surface of ELISA plate we optimized the binding conditions of the immobilization of MT onto the surface of our paramagnetic nanoparticles, which enable magnetic separation of protein for further immunolabeling with QDs@anti-MTAbs (entire workflow process is depicted in Fig. 2D). The binding recovery of MT was evaluated in the environment of different pH of borate buffers (5.0–7.0) and by using of DPV method it was shown that the best binding conditions are maintained in buffer with pH 6.0 (Fig. 2E with inset showing the voltammogram of MT, where Cat2 was employed for quantification according to our previous study [28]). The recovery of MT (500 nM) under optimized conditions was established to 24%. After we verified, that anti-MT abs are usable for the MT quantification in real samples using direct ELISA protocol, despite the general fact that certain Abs may be unsuitable for direct labeling, we decided to follow direct ELISA protocol to reduce number of operations, which will be carried out in the PDMS chip.

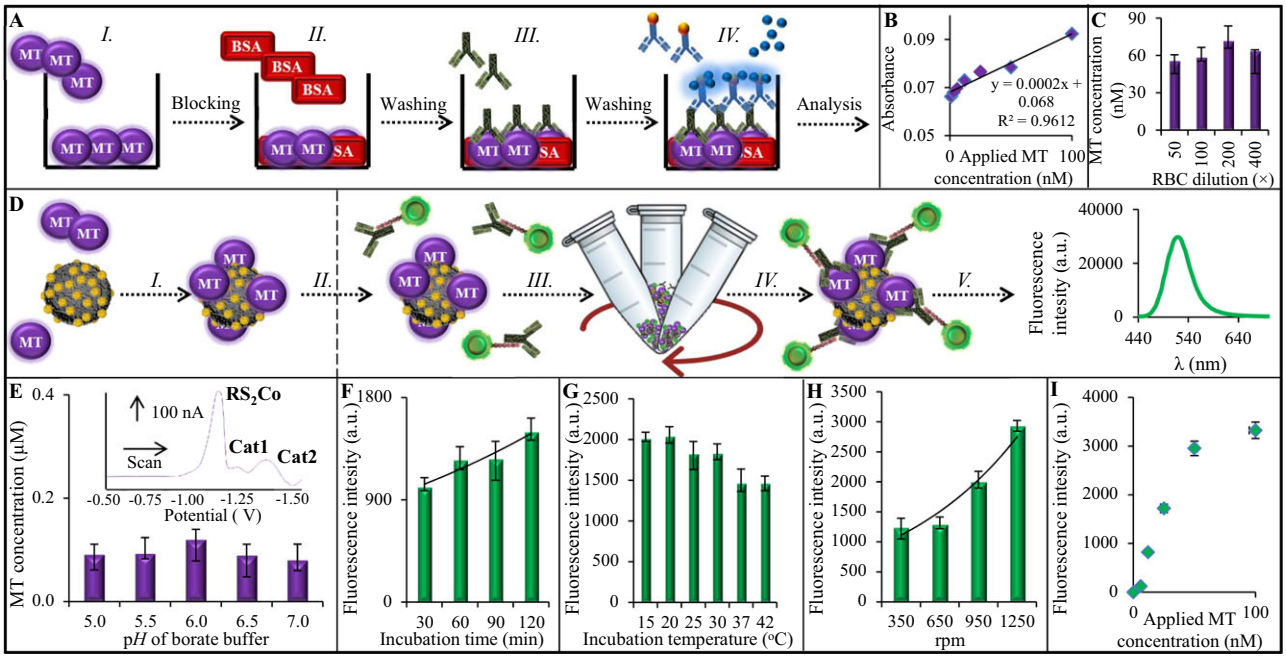

Figure 2. (A) Overall schematic depiction of direct ELISA of MT. (*I.*) The bottom of ELISA plate well was coated with MT (100 μL). After washing, the unoccupied surface of bottom was blocked by using 1% BSA (*II.*). Followed incubation with primary antibody (*III.*) and washing and binding of enzyme-linked secondary antibody, washing and addition of chromogenic substrate (*IV.*). (B) Calibration curve of standard of MT (1.3–100.0 nM), obtained through direct ELISA. (C) Method was applied to determine the MT levels in human red blood cells (RBC) (dilutions 1:50–1:500). (D) Schematic depiction of MT binding on surface of modified paramagnetic nanoparticles (*I.*) with immunolabeling by QDs@Anti-MTAbs (*II.*; *III.; IV.*). After immunoconjugation, fluorescence of complex was determined by using fluorescence spectroscopy (*V.*). (E) Optimization of ideal binding conditions (pH of borate buffer) of MT (500 nM) on paramagnetic nanoparticles, determined by DPV Inserted is voltammogram of MT (in borate buffer with pH 6) with typical catalytic peaks. Optimization steps for the largest yield of immunolabeled MT (applied concentration 500 nM) bound on paramagnetic nanoparticles, starting with (F) optimization of incubation time, (G) optimization of incubation temperature, (H) optimization of RPM during incubation. (I) Calibration curve of MT (6–100 nM). Values are means of three independent replicates ($n = 3$). Vertical bars indicate standard error.

In the preliminary tests, it was shown that direct labeling of anti-MTAbs enables their further application; however, fluorescence yields were relatively low (data not shown) and optimizations were required. Firstly, we suggested that incubation time may play the key role in efficiency of immunolabeling and it was shown that 120 min incubation enhanced the fluorescence intensity (1500 a.u.) when compared to 30 min (1010 a.u.; Fig. 2F). Long incubation permits a better coating of free MT on the solid phase and is necessary for the binding between MT and antibodies, especially while analyzing low concentrations [29]. Prolonged incubation beyond the tested range increased the fluorescence yields marginally. Thus with regards to the prolonging of overall operation time it would be unsuitable for application in biosensors. The second parameter influencing the immunoassay performance was the incubation temperature (range 15–42°C) with applied incubation time of 120 min. As it can be seen in Fig. 2G, the largest efficiency of MT immunolabeling was observed after incubation at 20°C (2040 a.u.), whereas lower (15°C) as well as higher temperatures (25–42°C) exhibited a reduction of fluorescence intensity (2000 a.u. at 15°C, 1460 a.u. at 42°C, respectively). After obtaining both, temperature and time, we optimized the last parameter—revolution per minute (rpm), which describes the shaking rate during incubation (120 min, 20°C; Fig. 2H), while the highest immunolabeling yields were observed at 1250 rpm (2930 a.u.). Interestingly, this parameter influences the resulting fluorescence the most, probably due to the mediation of dispersion of relatively heavy QDs@Anti-MTAbs, which than easily interact with the MT on the paramagnetic nanoparticles. Finally, by using the optimized conditions calibration curve of MT (6–100 nM) was established (Fig. 2I).

3.3 3D-printed platform for sensing of MT via QDs@anti-MTAbs fluorescence intensity

After optimization of important conditions we decided to employ our immunolabeling approach in 3D-printed biosensor with PDMS chip. The printing material was polymer acrylonitrile butadiene styrene, since a distinct advantage of using polymers is particularly the possibility of choice of material with specific chemical and physical properties (such as optical transparency, chemical resistance, stiffness, critical surface tension, etc.) [30]. As a substrate for crafting the chip with reservoir for ELISA performance we utilize PDMS. Besides good biocompatibility, PDMS has a perfect elastic characteristics and excellent optical attributes, thus it can facilitate the application of common optical measuring technologies [32]. Figure 3A shows the separate parts of the biosensor, Fig. 3B

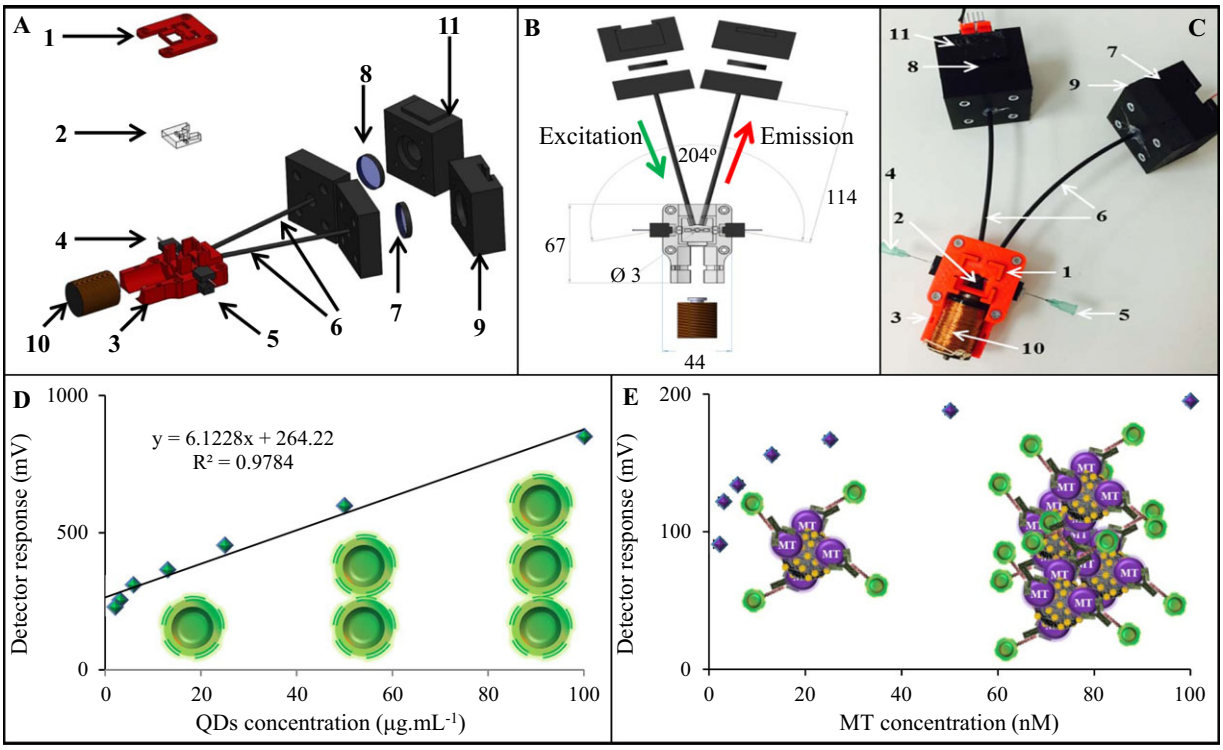

Figure 3. (A) Schematic depiction of biosensor device employed for MT magnetic separation and immunolabeling, where 1 stays for part, covering the PDMS chip, 2 for PDMS chip (with reservoir with volume of 50 μL) for magnetic separation and immunolabeling, 3 holder for PDMS chip, 4 fluidic inlet, 5 fluidic outlet, 6 optical fibers leading to excitation source and emission detector, 7 emission optical filter 550(55) nm, 8 excitation optical filter shortpass (425 nm), 9 emission detector with photodiode, 10 electromagnet for immobilization of magnetic nanoparticles, 11 LED source of excitation. (B) Schematic drawing of biosensor with expression of dimensions (mm) and optical light path of excitation and emission and (C) its photo. (D) Calibration curve of CdTe QDs (3.0–100.0 μg/mL), measured in biosensor. (E) Calibration curve of MT standard (2.0–100.0 nM), determined in biosensor, by using magnetic separation and detection by QDs-HWR-anti-MTAbs.

shows a schematic drawing of biosensor with important dimensions (mm), and Fig. 3C represents photography of the assembled device prior measurements.

First, for a confirmation of proper functionality of biosensor detection system we analyzed the bare QDs (2–100 μg/mL) to observe the dependence of the detector response on the QDs concentration. Samples of QDs were injected through the inlet into the PDMS reservoir and measurements were carried out immediately, whereas for perfect washing out of sample from reservoir (no fluorescence signal observed) was used ACS water (500 μL). Figure 3D shows the raw data, obtained from measurements and it is obvious that detector responded linearly to the applied amount of QDs ($y = 6.1228x + 264.22$, $R^2 = 0.9784$), and thus it can be applied for in-chip immunolabeling of MT. As the conditions of ELISA were optimized in previous steps, we followed them in our workflow process, where first, washed paramagnetic nanoparticles (0.5 mg/100 μL, vol. 100 μL) were immobilized in the PDMS chip by using an electromagnet and washed with 100 μL of borate buffer (pH 6) three times to remove undesired impurities. The standard of MT (3–100 nM) was injected in the volume of 100 μL to fill the reservoir and incubation was carried out under the optimized conditions (electromagnet operated at frequency 48 kHz, to imitate 800 rpm). After 30 min, the unbound MT was washed out three times with 100 μL of borate buffer with 0.5% Tween-20 and 1% BSA and subsequently 100 μL of solution containing QDs@anti-MTAbs was flushed inside PDMS chip. After incubation under the optimized conditions (electromagnet operated at frequency 72 kHz, to imitate 1250 rpm), the unconjugated QDs@anti-MTAbs were washed out with 100 μL of QDs-compatible borate immunobuffer and finally the fluorescence of QDs was determined. In Fig. 3E, a resulting curve, describing the dependence of detector response on the amount of conjugated QDs@anti-MTAbs is shown. The shape of the curve in the concentration range 50–100 nM indicates that paramagnetic nanoparticles probably depleted their capacity for protein binding, thus in concentrations higher than 50 nM the plateau was observed, which is in agreement with our optimization experiment, where the similar behavior of nanoparticles-MT-QDs@anti-MTAbs conjugate was observed (Fig. 2I).

3.4 Determination of MT in spinocellular carcinoma and fibroblast cell lines

The main aim of our study was to develop the portable device with ability to quantify the MT content in real samples. Main motivation was particularly the potential

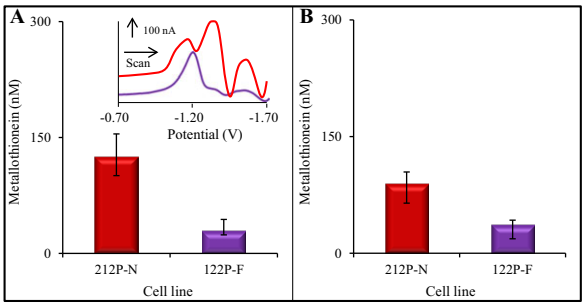

Figure 4. Determination of MT content in two cell lines — spinocellular carcinoma cells 212P-N and human fibroblasts 122P-F, determined by using (A) DPV, with inset showing corresponding voltammograms. (B) 3D-printed biosensor, based on in-chip immunolabeling of MT. Values are means of three independent replicates ($n = 3$). Vertical bars indicate standard error.

of MT to serve as a diagnostic biomarker of spinocellular carcinomas [3]. Such biosensor might be helpful while rapid screening evaluation of MT levels is required without need of immunohistochemistry or instrumentation for conventional ELISA. For comparison of functionality of our developed biosensor we decided to employ DPV, which we commonly use for MT quantification in various biological matrixes with high sensitivity [12, 28, 31]. As it is shown in Fig. 4A, by using DPV, the levels of MT in cell lysates were established to be 126 nM in 212P-N (derivate from spinocellular carcinoma) and 29 nM in 122P-F (human fibroblasts). By using our developed biosensor, the levels of MT were found to be 90 nM in 212P-N and 37 nM in 122P-F, respectively (Fig. 4B). The discrepancy between DPV and 3D-printed biosensor in the case of spinocellular carcinoma cells was established to be about-29%. As it was shown in our previous study, dealing with comparison of MT ELISA and DPV, the content of MT in fish tissue determined by using immunoassay reached approximately 75% of amount of MT analysed by DPV [14]. It is linked with the methods principles — whereas DPV determine total thiols, antibodies recognize directly target protein, however the immunoreactivity toward various MT isoforms can be lower than toward MT2 used for immunization of chickens. Developed biosensor is able to determine the MT concentrations, which can discriminate the spinocellular tumor cells from nontumor fibroblasts with advantages such as low-volume requirements ($< 100\ \mu L$), low acquisition costs when compared with full ELISA facility, and portability.

4 Concluding remarks

In particular, because of low fabrication cost, low material consumption and portability, biosensors have currently attracted much attention. In this study, we developed 3D-printed biosensor with PDMS chip that could be employed for magnetic separation of MT as the biomarker of various types of cancer, including spinocellular carcinoma. The isolation provided by magnetic nanoparticles offers suitable and inexpensive approach for sample pre-treatment prior to detection, because of elimination of undesired interferents, present in the real samples. Detection based on quantum dots combined with antibodies couples the perfect specificity of recognition elements–antibodies, with quantum dots outstanding quantum yields useful for such applications. Thus, our biosensor might be helpful when rapid screening evaluation of MT levels is required without need of immunohistochemistry or instrumentation for conventional ELISA.

Financial support by SPINCANCER NT/14337 is highly acknowledged. The authors wish to express their special thanks to Dagmar Uhlirova for perfect technical assistance.

The authors have declared no conflict of interest.

5 References

[1] Yang, Z. Y., Sweedler, J. V., *Anal. Bioanal. Chem.* 2014, *406*, 4013–4031.

[2] Kim, N., Son, S. H., Kim, W. Y., *Sens. Actuator B-Chem.* 2014, *198*, 157–163.

[3] Gumulec, J., Raudenska, M., Adam, V., Kizek, R., Masarik, M., *PLoS One* 2014, *9*, 1–14.

[4] Theocharis, S., Klijanienko, J., Giaginis, C., Rodriguez, J., Jouffroy, T., Girod, A., Point, D., Tsourouflis, G., Sastre-Garau, X., *Histopathology* 2011, *59*, 514–525.

[5] Sochor, J., Hynek, D., Krejcova, L., Fabrik, I., Krizkova, S., Gumulec, J., Adam, V., Babula, P., Trnkova, L., Stiborova, M., Hubalek, J., Masarik, M., Binkova, H., Eckschlager, T., Kizek, R., *Int. J. Electrochem. Sci.* 2012, *7*, 2136–2152.

[6] Iszard, M. B., Liu, J., Klassen, C. D., *Toxicology* 1995, *104*, 25–33.

[7] Namdarghanbari, M., Wobig, W., Krezoski, S., Tabatabai, N. M., Petering, D. H., *J. Biol. Inorg. Chem.* 2011, *16*, 1087–1101.

[8] Shibuya, K., Nishimura, N., Suzuki, J. S., Tohyama, C., Naganuma, A., Satoh, M., *J. Toxicol. Sci.* 2008, *33*, 651–655.

[9] Heger, Z., Zitka, O., Fohlerova, Z., Rodrigo, M. A. M., Hubalek, J., Kizek, R., Adam, V., *Chemical Papers* 2014, *33*, 54–61.

[10] Kim, N., Shon, S. H., Kim, C. T., Cho, Y. J., Kim, C. J., *Curr. Appl. Phys.* 2011, *11*, 1210–1214.

[11] Janu, L., Stanisavljevic, M., Krizkova, S., Sobrova, P., Vaculovicova, M., Kizek, R., Adam, V., *Electrophoresis* 2013, *34*, 2725–2732.

[12] Skalickova, S., Zitka, O., Nejdl, L., Krizkova, S., Sochor, J., Janu, L., Ryvolova, M., Hynek, D., Zidkova, J., Zidek, V., Adam, V., Kizek, R., *Chromatographia* 2013, *76*, 345–353.

[13] Krizkova, S., Adam, V., Eckschlager, T., Kizek, R., *Electrophoresis* 2009, *30*, 3726–3735.

[14] Krizkova, S., Blahova, P., Nakielna, J., Fabrik, I., Adam, V., Eckschlager, T., Beklova, M., Svobodova, Z., Horak, V., Kizek, R., *Electroanalysis* 2009, *21*, 2575–2583.

[15] Tmejova, K., Hynek, D., Kopel, P., Krizkova, S., Blazkova, I., Trnkova, L., Adam, V., Kizek, R., *Colloid Surf. B-Biointerfaces* 2014, *117*, 534–537.

[16] Zitka, O., Cernei, N., Heger, Z., Matousek, M., Kopel, P., Kynicky, J., Masarik, M., Kizek, R., Adam, V., *Electrophoresis* 2013, *34*, 2639–2647.

[17] Zitka, O., Heger, Z., Kominkova, M., Skalickova, S., Krizkova, S., Adam, V., Kizek, R. *J. Sep. Sci.* 2014, *37*, 465–475.

[18] Zhu, X. S., Duan, D. Y., Madsen, S., Publicover, N. G., *Anal. Bioanal. Chem.* 2010, *396*, 1345–1353.

[19] Zitka, J., Heger, Z., Cernei, N., Michalek, P., Krizkova, S., Kopel, P., Masarik, M., Hodek, P., Zitka, O., Adam, V., Kizek, R., *J. Met. Nano.* 2014, in press.

[20] Long, G. L., Winefordner, J. D., *Anal. Chem.* 1983, *55*, 712–724.

[21] Saito, S., Kurasaki, M., *Res. Commun. Mol. Pathol. Pharmacol* 1996, *93*, 101–107.

[22] Zhou, M., Wang, B. X., Rozynek, Z., Xie, Z. H., Fossum, J. O., Yu, X. F., Raaen, S., *Nanotechnology* 2009, *20*, 1–7.

[23] Schwegmann, H., Feitz, A. J., Frimmel, F. H., *J. Colloid Interface Sci.* 2010, *347*, 43–48.

[24] Qu, L. H., Peng, X. G., *J. Am. Chem. Soc.* 2002, *124*, 2049–2055.

[25] Sapsford, K. E., Pons, T., Medintz, I. L., Mattoussi, H., *Sensors* 2006, *6*, 925–953.

[26] Martin-Yerga, D., Gonzalez-Garcia, M. B., Costa-Garcia, A., *Talanta* 2014, *130*, 598–602.

[27] Puertas, S., Batalla, P., Moros, M., Polo, E., del Pino, P., Guisan, J. M., Grazu, V., de la Fuente, J. M., *ACS Nano* 2011, *5*, 4521–4528.

[28] Ryvolova, M., Hynek, D., Skutkova, H., Adam, V., Provaznik, I., Kizek, R., *Electrophoresis* 2012, *33*, 270–279.

[29] Kim, J., Rho, T. H. D., Lee, J. H., *Talanta* 2014, *129*, 106–112.

[30] Waldbaur, A., Rapp, H., Lange, K., Rapp, B. E., *Anal. Methods* 2011, *3*, 2681–2716

[31] Hung, L. H., Lin, R., Lee, A. P., *Lab Chip* 2008, *8*, 983–987.

[32] Adam, V., Petrlova, J., Wang, J., Eckschlager, T., Trnkova, L., Kizek, R., *PLoS One* 2010, *5*, 1–8.

